CO12-1   Study on Superposition of Coherent Transition Radiation Using a Ring Resonator

N. Sei, T. Takahashi[1]

Research Institute for Measurement and Analytical Instrumentation, National Institute of Advanced Industrial Science and Technology
[1]Institute for Integrated Radiation and Nuclear Science, Kyoto University

Fig. 1   Schematic layout of the ring-type resonator.

INTRODUCTION: As peak power of light sources in the terahertz (THz) region increase notably, novel applications using THz lights are pioneered to solve various issues. THz lights are no longer just probe lights for inspections. It has been reported that a THz light beam causes dissolution of a fibrous peptide [1], and it is expected that the THz light beam is applied to a new treatment technology. Developments of intense THz light sources will become increasingly important.

A key technique for increasing power of light pulses is to superimpose the electromagnetic field of the light pulses. We have confirmed that coherent diffraction radiation nonlinearly amplifies at resonant frequencies by using periodical diffractors [2]. In order to further develop this technique, we have experimented with confining and superimposing coherent radiation generated by a pulse train of electron bunches in a ring-type resonator. Although a resonant light extracted from the ring-type resonator though a coupling hole of a mirror was observed, a background level of coherent diffraction radiation was high. Therefor, in order to decrease the background, we performed experiments with a thin substrate inserted in the resonator as a coupling device.

EXPERIMENTS: The experiments were performed using an electron beam with the energy of 42 MeV and the macropulse duration of 47 ns in an L-band linac at Kyoto University Institute for Integrated Radiation and Nuclear Science. The repetition frequency of the macropulse of the electron beam was 30 Hz. Schematic layout of the ring-type resonator used in the experiments is shown in Fig. 1. The electron beam generated coherent transition radiation (CTR) at two thin polyethylene films vapor-deposited with aluminum when it passed through them. The thickness of the polyethylene film was 6 μm. The current of the electron beam passed through the polyethylene film was approximately 60 μA. These polyethylene films were also used as mirrors constituting the ring resonator. The two CTR beams were confined in the ring resonator composed of four mirrors, which included two parabolic mirrors with the focal length of 508 mm. The length of the resonator was 922 mm, which was four times the interval of the electron bunches. In order to extract the resonate CTR beam from the optical cavity, a ZEONEX substrate with a thickness of 3 mm was inserted into the resonator at an angle of 45 degrees with respect to the optical axis. The ZEONEX was almost transparent i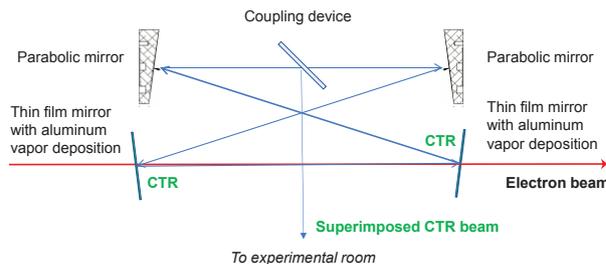n a frequency range below 1 THz, and its refractive index was 1.53. Although the CER was reflected on both sides of the substrate, the two reflected beams did not interfere due to the thickness of the substrate.
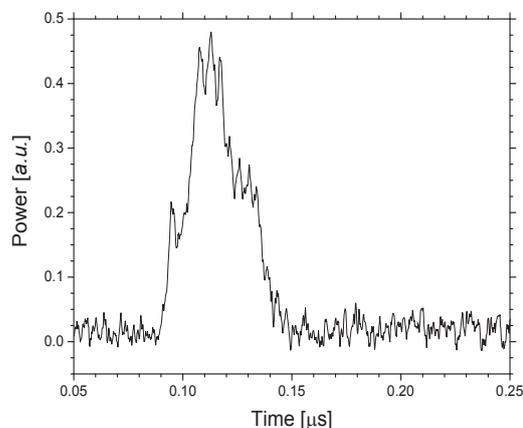

Fig. 2   Measured CTR power extracted from the ring-type resonator in the D-band.

RESULTS: The CTR beam transported to the experimental room was measured by a D-band diode detector (Militech Inc., DXP-06). As shown in Fig. 2, several peaks were observed in the macropulse of the measured CTR power but did not have periodicity. Because micropulse structure of the CTR beam disappeared in the macropulse, it was considered that the ring-type resonator deviated from the resonance condition. By adjusting position of a stage on which the parabolic mirror was installed, the resonance conditions could have been improved. Moreover, it was difficult to detect detailed structure in the macropulse due to the low CTR power. To increase efficiency of CTR extraction from the resonator, we consider using a material with a high refractive index as the coupling device. We also plan to use thin coupling device so that the reflected CTR beams on the both sides of the coupling device can be coherent.

REFERENCES:
[1] T. Kawasaki *et al*., Sci. Rep. **9** (2019) 10636.
[2] N. Sei and T. Takahashi, Sci. Rep. **10** (2020) 7526.

R2013

CO12-2 **Empirical Research on the Effective Introduction and Unification of Ambient Dose Rate Mapping Methods Using Car-borne Survey System for Monitoring of Nuclear Facilities by Local Governments**

H. Tanaka[1], M. Tanigaki[2]

[1]*Japan Chemical Analysis Center*
[2]*Institute for Integrated Radiation and Nuclear Science, Kyoto University*

INTRODUCTION: The car-borne survey of ambient dose rate is categorized by NRA (Nuclear Regulation Authority) as one of the monitoring methods in emergency situations at nuclear facilities. Therefore, it is important to effectively introduce and standardize the method for mapping the ambient dose rate measured by the car-borne survey conducted by local governments.

This time, we researched the nationwide unification of mapping procedure of carborne surveys. In this study, ambient dose rate maps obtained by KURAMA-II (Kyoto University Radiation Mapping system) [1] (Fig.1) were used.

EXPERIMENTS: The data for the mapping were measured using KURAMA-II in the several areas in Japan where the ambient dose rate levels are different:
(1) Data measured at around the TEPCO Fukushima Daiichi Nuclear Power Plant (Fukushima prefecture) [2]
(2) Data measured at low level areas of ambient dose rate level (Iwate prefecture and Shizuoka prefecture).

The acquired data were stored in the cloud server for KURAMA-II of Kyoto university, and each ambient dose rate map was created.

A questionnaire survey about effectiveness of each map was conducted to the staff of local governments who should be involved to car-borne surveys for monitoring nuclear facilities.

RESULTS: As shown in Fig. 2, ambient dose rate maps were created for each data.
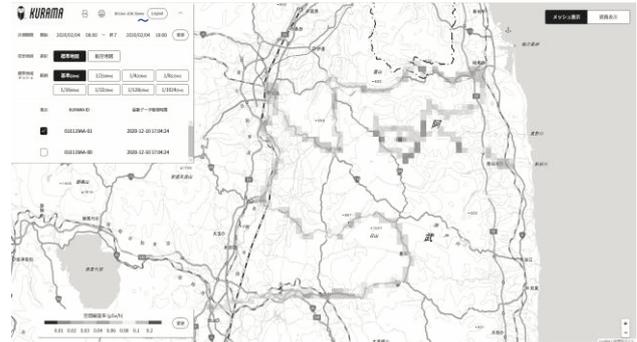

Fig.1 KURAMA-II.

Fig.2 Ambient dose rate map by data measured in Fukushima prefecture.

Nine responses were obtained from local government organizations and individuals belonging to them.
From the results of the questionnaire, the current ambient dose rate maps basically have essential information and functions required by the local government for emergency monitoring.
Followings are comments to the current ambient dose rate map. We continue to work for the improvements to the map based on these comments.

Information that should be implemented to the map
- Landmarks (public facilities such as schools and government offices, shelters, etc.)
- Distance display on concentric circles from nuclear facilities, distance scale, 16 directions. (It would be effective to be able to select display / non-display by selection.)
- Area display of nuclear disaster countermeasure priority areas (PAZ, UPZ, etc.)
- Boundary display of evacuation units

Functions that should be implemented to the map
- Cooperation with the national emergency radiation monitoring information sharing system
- Easy-to-read color of ambient dose rate display
- Spectrum display
- Easy-to-input of measurement period

REFERENCES:
[1] M. Tanigaki et al., Nucl. Instrum. Meth. **A781**(2015)57-64.
[2] Japan Chemical Analysis Center, Report of the survey of technical specifications with various carborne survey systems granted by NRA (2020).

R2033

CO12-3 Development of neutron imager based on hole-type MPGD with glass capillary plate

F. Tokanai[1], T. Moriya[1], T. Sumiyoshi[2], H. Kondo[3], H. Sugiyama[3], T. Okada[3], M. Hino[4], T. Oda[4]

[1]*Faculty of Science, Yamagata University*
[2]*Graduate School of Science, Tokyo Metropolitan University*
[3]*Electron Tube Division, Hamamatsu Photonics K. K.*
[3]*Institute for Integrated Radiation and Nuclear Science, Kyoto University*

INTRODUCTION: High position resolution with a moderate effective area is required in practical applications of neutron imaging. We have been developing a high-spatial-resolution neutron gas scintillation imager (n-GSI) with a capillary plate gas detector (CPGD) [1,2]. Fig. 1 shows a schematic view of the n-GSI. It consists of a $^{10}B_4C$ converter layer, a CPGD filled with a Ne (90%) + CF_4 (10%) gas mixture, a mirror, a lens optics, an imaging intensifier (I.I.) unit, and a CMOS camera. Neutrons passing through a sample enter the n-GSI. The $^{10}B_4C$ converter is directly mounted on the inlet surface of the CP. Charged particles (α-rays and ^7Li nuclei) are generated by a nuclear reaction between incident neutrons and ^{10}B. The charged particles ionize the gas molecules, resulting in the generation of electrons in the gas. Scintillation light is emitted from capillary holes upon gas excitation, simultaneously with electron multiplication. The scintillation light from each capillary is read out as the imaging signal through the optical mirror and lens system using an I.I. CMOS camera.

Since the ^{10}B converter is directly mounted on the inlet surface of the CP, the track length of the charged particles is restricted to within the capillary. Thus, the spatial resolution of incident neutrons is expected to be close to the capillary diameter. In this measurement, the imaging capability was investigated through comparison with a conventional neutron scintillation detector.
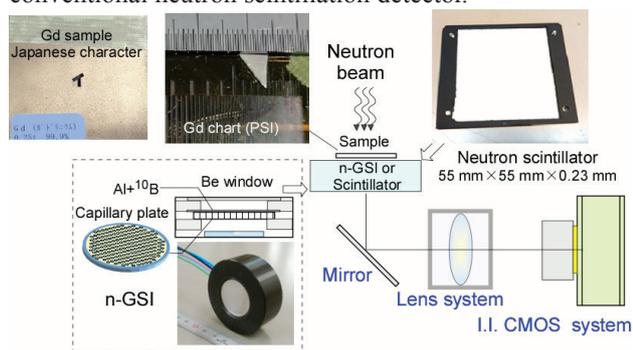

Fig. 1. Experimental setup of the n-GSI. A conventional neutron scintillation detector (NSD) is installed in place of the n-GSI.

EXPERIMENTS: The imaging capability of the n-GSI were investigated using the cold neutron beamline CN-3 installed at the Kyoto University Reactor (KUR) [3]. The neutron wavelength giving the maximum intensity and the total flux of the CN-3 guide tube were 2 Å and 3.8 × 10^6 neutrons cm^{-2} s^{-1}, respectively. The n-GSI system was placed 300 mm from the downstream exit of the neutron guide. The neutrons were irradiated into a sample. In this measurement, a conventional neutron scintillation detector (NSD) was installed in place of the n-GSI. and the performance test was conducted for comparison.

RESULTS: The neutron transmission images of a Japanese character and a Gd chart obtained with the n-GSI and the NSD are shown in Fig. 2 and Fig. 3, respectively. The exposure times for the images were 100 s. The image of the NSD is brighter than that of n-GSI. The light yield of the NSD, defined as the mean counts in the ROI, is about 2 times higher than that obtained by n-GSI. The contrast is expected to improve on applying a higher gap voltage across the CP since the light yield of the n-GSI increases exponentially with the gap voltage. Moderate imaging capabilities were evident from the two neutron images of the Gd chart. More detailed analysis is in progress.
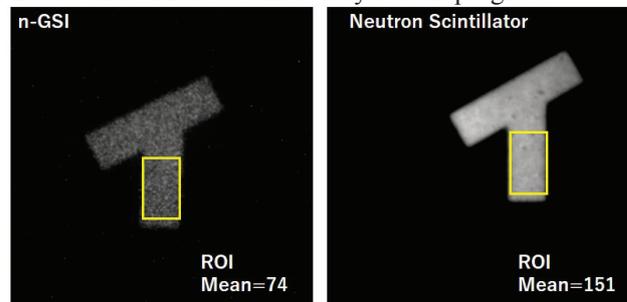

Fig. 2. Neutron transmission image of a Japanese character obtained using the n-GSI (left) and the NSD (right). The region of interest ROI (yellow) is defined to investigate the light yield of the neutron transmission image.
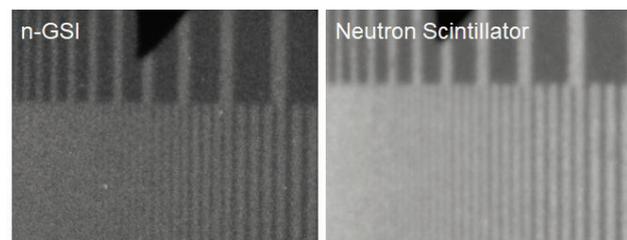

Fig. 3. Neutron transmission image of a Gd test chart obtained using the n-GSI (left) and the NSD (right).

REFERENCES:
[1] H. Kondo et al., Plasma Fusion Res. 13 (2018) 2406018.
[2] H. Kondo et al., Nucl. Instrum. and Methods. A 958 (2020) 162804.
[3] H. Sugiyama et al., IEEE Trans Nucl Sci. 67 (2020) 1035.
[4] M. Hino et al., Nucl. Instrum. and Methods. A 797 (2015) 265.

R2036

CO12-4   Stability Monitoring of Hf Oxide Films by Neutron Activation Analysis

T. Takatsuka, K. Hirata, Y. Iinuma[1], R. Okumura[1],
H. Yoshinaga, and K. Takamiya[1]

National Metrology Institute of Japan, National Institute of Advanced Industrial Science and Technology
[1]Institute for Integrated Radiation and Nuclear Science, Kyoto University

INTRODUCTION: Hafnium (Hf) oxide is utilized as high-*k* dielectric films for semiconductor devices especially with fast and low-power operation. Additionally, the films are being introduced as ferroelectric material on ferroelectric transistors and memories. The device fabrication process should be precisely controlled for such dielectric films. Certified reference material NMIJ-CRM 5605-a was developed in 2012 [1, 2], which is applicable to quantify the film thickness with small uncertainties. This study aims to confirm the stability of hafnium quantity in thin hafnium oxide films by neutron activation analysis (NAA), to keep the reliability of the certified reference material.

EXPERIMENTS: Hf oxide films were deposited on 4-inch Si wafers by magnetron sputtering. The target thickness was set to 4 nm. The prepared wafers with the films were cut into 10 mm × 10 mm pieces for the measurements. The surface areas of specimens were precisely calculated from the optically scanned images, with the length calibration using JCSS calibrated standard scales.

Hafnium amounts were evaluated by NAA with internal standards. For the production of standards to calibrate hafnium amounts, standard solutions were prepared by diluting NIST SRM 3122: Hf and 3102: Sb gravimetrically. Four concentration levels of working standard solutions were prepared: an internal standard solution of Sb, three Hf and Sb mixed standard solutions with different Hf concentrations for the calibration. Weighed portion of the Sb working standard solution was dropped onto a cleaned filter paper on every specimen. As for standards, aliquots of the working standard solutions of Hf and Sb mixture were weighed and dropped onto filter papers.

All the samples were sealed up separately in clean polyethylene bags, followed by being stacked in a polyethylene container for the neutron irradiation. The irradiation was performed for 4 hours with a 5.5×10^{12} cm^{-2}·s^{-1} thermal neutron fluence rate at Pn-2 in the Kyoto university research reactor (KUR). The gamma-ray activity of each sample was measured by a high-purity germanium detector (CANBERRA).

RESULTS: From the gamma-ray spectrum, the gamma-ray relative intensities (^{181}Hf cps) / (^{124}Sb cps/ ng) were calculated for the specimens and the standards. Figure 1 shows typical calibration curve plotting the relative intensities to the Hf amounts. The hafnium content in each specimen was estimated from the calibration curve.

Dividing each Hf amount by the measured surface area,

the area density was calculated for each measured specimen. The evaluated area densities of CRM 5605-a specimens are plotted with the uncertainty (error bars), in Fig. 2, the horizontal axis shows when the measurements were conducted in year and month. The area densities consistent with each other when considering the uncertainties. This result shows the stability of hafnium quantity in thin hafnium oxide films on the CRM.
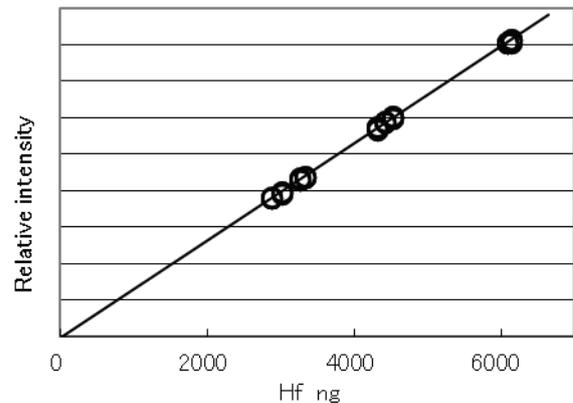

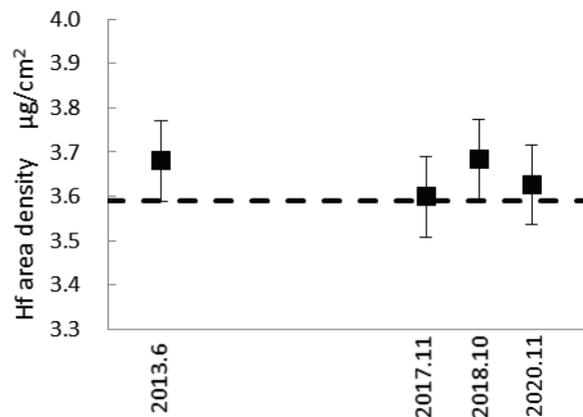Fig. 1. Calibration curve for determining the Hf contents by the internal standard method.

Fig. 2. Stability monitoring of the Hf area density by the internal standard method. The broken line indicates the certified value of CRM 5605-a.

REFERENCES:
[1] Certificate of NMIJ CRM 5605-a: Hafnium Oxide Film for Quantitative Analysis of Hafnium.
[2] KURRI Progress Report 2012.

R2038

Neutron irradiation test at KUR CN-3

H. Ohshita, H. Endo, T. Seya, Y. Yasu, M. Hino[1], T. Oda[1]

Institute of Materials Structure Science, KEK
[1]Institute of Integrated Radiation and Nuclear Science, Kyoto University

INTRODUCTION: Kyoto University Research Reactor (KUR) is a light-water moderated tank-type reactor with a thermal power of 5 MW. The cold neutron beam line (CN-3) [1] is built facing the direction of the cold neutron moderator of the KUR. Neutrons between 1 Å and 6 Å are led by neutron supermirror guides to the experimental area. The total length of the CN-3 is 10.5 m. The neutron supermirror guide consists of 15 elements with a length of 70 cm each. In addition, the guide has a curvature radius of 441 m. Furthermore, the CN-3 is curved at the carry-in entrance. Therefore, fast neutrons are not able to reach the experimental area. The beam corresponds to the size of the neutron supermirror guide and has a height of 90 mm and a width of 20 mm. Because neutrons with garland reflection have a shorter wavelength than those with zigzag reflection, the outside (SANS side) component that has many neutrons with garland reflection shifts to a shorter wavelength than that of the inside (the carry-in entrance side) component. Currently, the cold neutron moderator is nonfunctional. The expected neutron intensity is 7.6×10^5 neutrons/s·cm^2·MW. We carried out the neutron irradiation test at the KUR CN-3 in addition to developing some neutron detectors. In this study, we will discuss the neutron yield of CN-3.

EXPERIMENTS AND RESULTS: An experimental setup for the measurement of neutron intensity is shown in Figure 1. An L-shaped neutron shield is placed around the beam duct. A movable slit, neutron beam monitor, and disk chopper with a ϕ500 mm disk are set on the inside. A ^{3}He filled proportional counter is also set on the outside. The fixed movable slit has a height of 20 mm and a width of 10 mm. The neutron beam monitor (MNH10/4.2), which is filled with little amounts of ^{3}He and P-10 gases, attains a neutron efficiency of order 10^{-4}. The total pressure of the monitor is 130 kPa. The typical counting rate is approximately 218.4 events/s·MW and is used as the normalization factor. Heavy neutron irradiation with a continuous beam is carried out upstream of the chopper. A composite board with a ^{6}LiF tile (5 mm$t$) and a Cd plate (1 mm$t$) is set as the fixed collimator for the chopper. The chopper has adjustable slit sizes of 0.5 mm, 1 mm, 5 mm, and 40 mm. The chopper has four openings and a rotation rate of 30 Hz. The neutron shield of the chopper consists of a B$_4$C rubber (6 mm$t$) and a Cd plate (2 mm$t$). Time-of-flight (TOF) measurement is carried out downstream. In simple Monte Carlo simulation, the expected neutron intensity with a slit size of 1 mm width is 937.4 neutrons/s·cm^2·MW. In the simulation, only the geometrical condition and movement of the chopper are considered. The ^{3}He filled proportional counter (RS-P4-0806-264) covered with a B$_4$C resin

shield is used to measure the TOF. The counter has a gas mixture of ^{3}He and CO$_2$ (99:1), and the total pressure is 1003.19 kPa. The counter is cylindrical in shape with a 1 inch diameter. The opening area of the B$_4$C resin shield is 10 mm × 10 mm. As the measurement results, the neutron beam scan by moving the counter laterally from the carry-in entrance side is shown in Figure 2. The effect between garland and zigzag reflections is illustrated. The neutron intensity is estimated as 694.5±0.5 neutrons/s·cm^2·MW, as shown in Figure 3. To understand the difference between the measurement and the simulation, we plan to realign neutron optics. This study was carried out in part under the support of JSPS KAKENHI; Grant Numbers JP20K12503 and JP20H04462.

REFERENCES:
[1] M. Hino, *et al.*, Annu. Rep. Res. Reactor Inst. Kyoto Univ. **27** (1994) 196-204.
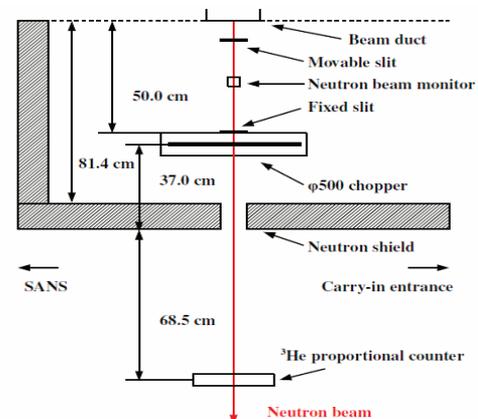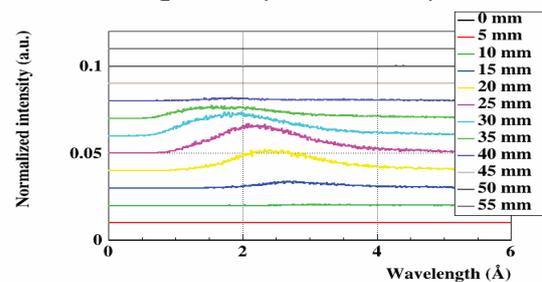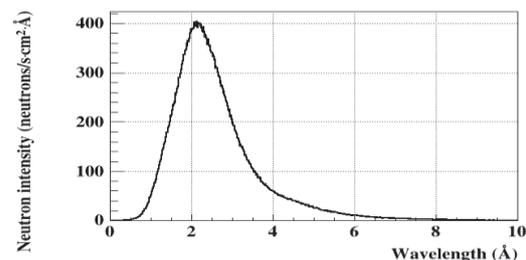

Figure 1 Experimental setup.

Figure 2 Neutron beam scan.

Figure 3 Neutron intensity.

R2069

CO12-6   A Study of Polyvinylalcohol-borate hydrogels using small angle X-ray scattering

T. Tominaga[1], Y. Sasaki[2], H. Seto[2], R. Inoue[3], N. Sato[3], and M. Sugiyama[3]

[1]Neutron Science and Technology Center, Comprehensive Research Organization for Science and Society (CROSS)
[2]Institute of Materials Structure Science / J-PARC Center, High Energy Accelerator Research Organization, Tokai, Japan
[3]Institute for Integrated Radiation and Nuclear Science, Kyoto University

INTRODUCTION: One of the features of soft matter is that it undergoes great deformation. Polyvinylalcohol-borate hydrogels (so called 'slime') composed of polyvinylalcohol (PVA), borax and water has long been known as a toy are a soft matter that is known to undergo great deformation. As the amount of borax increases, the hydrogels become less deformed. On the other hand, when the amount of borax is reduced, the PVA hydrogels can be deformed, it becomes soft but does not stretch.

When various additives are added to the hydrogels, the hydrogels become stretchable. One is glycerin, and the other is vinyl acetate granular resin (size: approximately 5 μm) with PVA chains on surface. These are substances with hydroxyl groups like PVA. It is considered that they reduce friction between PVA chains when stretching, but the details are unclear.

In this experiment, the structural change of PVA hydrogels by the addition of borax and vinyl acetate resin was confirmed by small angle X-ray scattering (SAXS).

EXPERIMENTS: PVA hydrogels were prepared in the following weight ratios: PVA: 6.5%, glycerin: 3.6%, borax: 0.4%, vinyl acetate granular resin and: 1.8% water: 88%. The amount of borax was kept constant for all hydrogels, and samples without glycerin, without borax, and without glycerin and borax were prepared. The hydrogels thickness was 0.8 mm and sandwiched between a polyetherimide resin (Sperio, Mitsubishi, Japan). The Cu-SAXS (RIGAKU Nanopix) available at Institute for Integrated Radiation and Nuclear Science, Kyoto University of high-resolution mode was utilized. The empty container was subtracted to account for the transmission, and the SAXS profile was obtained by circular averaging.

RESULTS: SAXS profiles of PVA hydorgels are shown in Fig. 1. The PVA hydrogels without both glycerin and vinyl acetate granular resin had a homogeneous structure at $Q < 10^{-2}$ Å^{-1}, while the hydrogels containing the additives was inhomogeneous in this Q region.

PVA is known to be a crystalline polymer and the structure observed at about $3–8 \times 10^{-2}$ Å^{-1} is considered to be an ordered structure due to the crystalline nature of PVA [1]. This structure appeared to shift toward a larger Q with the addition of additives, i.e., the crystal size becamed smaller.

The additives contributed significantly to the local homogeneity of PVA hydrogels. On the other hand, the inhomogeneity increased in the macroscale structure. This indicates that the crystal structure has a negative effect on the sliding property between the polymer chains, therefore reducing the crystal size improves the sliding property locally, and reducing the friction site number is consistent with mechanical properties of stretchable hydrogels, which in turn correlates with the inhomogeneous structure observed at large scale.

Although more detailed analysis is required, this is an important insight as a key point for the deformation of soft matters.
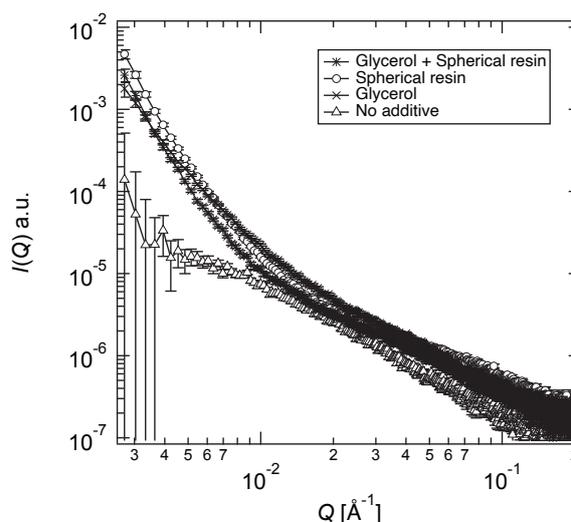

Fig. 1. SAXS profile of PVA hydrogels with PVA, water, and borax as common components. Both glycerin and spherical resin (*), only spherical resin (○), only glycerin (×), and none of the above (△)

REFERENCES:
[1] Toshiji Kanaya et al., Polymer Journal (2012) 44, 83–94 (2012).

R2073

CO12-7 Evaluation of LAN cable sheath degradation by gamma irradiation

Taiki Tominaga[1], Toshiyuki Chatake[2], Takeshi Saito[2], Nobuhiro Sato[2], Rintaro Inoue[2], Masaaki Sugiyama[2]

[1]Neutron Science and Technology Center, Comprehensive Research Organization for Science and Society (CROSS)
[2]Institute for Integrated Radiation and Nuclear Science, Kyoto University

INTRODUCTION: A light yellow liquid was found in the vacuum scattering chamber where the neutron detector is installed at the J-PARC MLF BL02 spectrometer [1]. The substance was evaluated and found to be plasticizers for polyvinylchloride cable sheaths such as dioctylphthalate, dinonylphthalate and didecylphthalate. Content ratio of these plasticizers vary from application to application, but generally account for 35–40% of the polyvinylchloride (PVC) cable sheathing [2]. Because these compounds contaminate the vacuum vessel and may be a factor to increase the background in the data of neutron experiments, a prompt investigation of the mechanism is necessary.

PVC sheathed cables are often used for LAN (Local Area Network) cables. Therefore, the possibility of plasticizer elution under vacuum and the possibility of plasticizer elution due to cable sheath degradation by gamma irradiation were evaluated by examining the change in weight before and after vacuum treatment and the change in Young's modulus before and after gamma irradiation.

EXPERIMENTS: Three types of commercial PVC LAN cables and two types of polyolefin (PO) LAN cables were prepared. The LAN cable has a double sheath structure, in which eight conductors are strung together two by two, and then they are loosely combined into one outer cable sheath. In this experiment, only the outer cable sheath was taken as a sample. The weight change was calculated as the average of three values under each condition, and the weight change was evaluated before and after vacuum treatment at 60°C, 5 Pa, for 5 h, and before and after gamma irradiation. The gamma irradiation experiments were conducted at the Co-60 Gamma-ray Irradiation Facility in the Institute for Integrated Radiation and Nuclear Science, Kyoto University. The samples were irradiated with 1 kGy gamma rays at a dose rate of 5 Gy/min in air. Cable sheaths were cut into 4 mm wide strips and tensile tested; the slope of the strain from 1 to 3% was analyzed, and the average value of the three test results was used as Young's modulus.

RESULTS: The weight loss of all cable sheaths unirradiated with gamma radiation was less than 0.1%. This suggests the additives such as plasticizers, flame retardants, etc. in the cable sheaths do not flow out simply by vacuum treatment. Next, the gamma-irradiated samples were further vacuum-treated, and the outflow of additives was evaluated from the weight change. Similarly, the weight change was less than 0.1%. The weight of the gamma-

irradiated samples increased slightly, suggesting that the gamma-irradiation had a slight effect on oxidation.
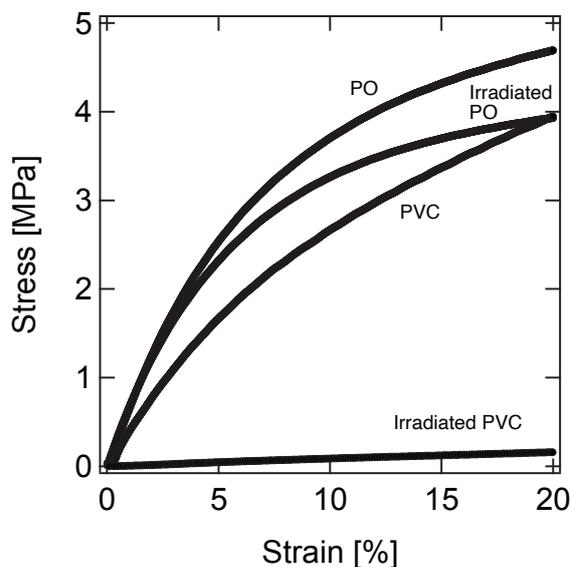

Fig. 1. Stress-strain curves of cable sheaths before and after gamma irradiation of a PVC sheath and a PO sheath.

Although there was no obvious trend in Young's modulus changes due to gamma irradiation between PO and PVC sheaths, both cable sheaths were damaged by gamma irradiation at a total dose of 1 kGy (Young's modulus decrease: 44–99% for PO sheaths and 2–72% for PVC sheaths). The s-s curves of the PO sheath with the smallest damage and the PVC sheath with the greatest damage are shown in Figure 1. The PO sheath cable with the minimum degradation due to gamma radiation is a non-halogenated cable available as eco-material (EM) cable, which may be affected by additives such as plasticizers and flame retardants in the cables, however the details are unclear.

The experimental results show that The 1 kGy dose of gamma radiation was insufficient to cause damage equivalent to that of the cable sheaths in the BL02 spectrometer. We are investigating the possibility of cable sheath degradation due to ultra-short-range irradiation caused by neutron absorption-induced activation.

REFERENCES:
[1] K. Shibata et al., JPS Conf. Proc. 8, 036022 (2015).
[2] R. Navarro et al., Macromolecules 43, 5, 2377–2381 (2010).

R2074

CO12-8   Competitive Adsorption Behaviour of Additives in Lubricating Oil Analyzed by Neutron Reflectometry

T. Hirayama, N. Yamashita[1], M. Hino[2], N. L. Yamada[3]

Dept. of Mechanical Eng. and Science, Graduate School of Kyoto University
[1]Dept. of Mechanical Eng. and Science, Graduate School of Kyoto University
[2]Institute for Integrated Radiation and Nuclear Science, Kyoto University
[3]Institute of Materials Structure Science, KEK

INTRODUCTION: General lubricating oil is a blend of base oil such as mineral oil and synthetic oil with additives, and it contributes to saving energy by reducing the friction loss of the machines. Therefore, among various additives, those having a friction reducing effect under boundary lubricated conditions are blended in the lubricating oil. However, the effect of additives when two or more kinds of additives are mixed in lubricating oil is still unknown. Classical textbook says that competitive adsorption of additives limits the improvement of friction reduction effect when several kinds of additives are mixed in lubricating oil together. Therefore, in this study, we investigated the structure of the adsorption layer and its coefficient of friction when fatty acids and alcohol, which are typical oiliness additives, were mixed in the base oil together, by using neutron reflectometry and atomic force microscope.

EXPERIMENTS:
For the structural analysis of adsorbed layer formed by additives, we used the time-of-flight (TOF) type neutron reflectometer SOFIA installed at the J-PARC in Tokai, Ibaraki. In order to grasp the film thickness and density of the boundary lubrication layer formed on the Cu surface in lubricant, we conducted fitting procedure for the obtained neutron reflectivity profiles in each case.

The base oil we used was hexadecane, and stearic acid and stearyl alcohol were used as a model of oiliness additives. We compared the neutron reflectivity profiles for two lubricants for checking the possibility of competitive adsorption by the combination use of additives; the first was with 0.1 mass% deuterated acid, while the second was with 0.05 mass% deuterated acid and 0.05 mass% deuterated alcohol.

RESULTS:
In the experiment, three neutron reflectivity profiles were obtained: (1) with base oil only, (2) immediately after the lubricant containing the additive was added, and (3) two hours after the lubricant containing the additive was added.

The obtained profiles are shown in Fig. 1. Since the width of the fringe in the reflectivity profile becomes wider as time goes by, it can be said that the total film thickness tended to become thinner. Since the extracted lubricant turned 'blue' after the experiment, it is probable

that the additive was adsorbed, causing corrosion of the Cu surface.

It can be seen that the change in fringe width was larger when the acid and alcohol were mixed than when the acid alone was used. This suggests that when stearic acid and alcohol were mixed, the corrosive action became greater, that is, the adsorption performance became higher than that of stearic acid alone. It was expected before the experiment that alcohol would suppress the adsorption of fatty acids and suppress corrosion, but the results showed the opposite.
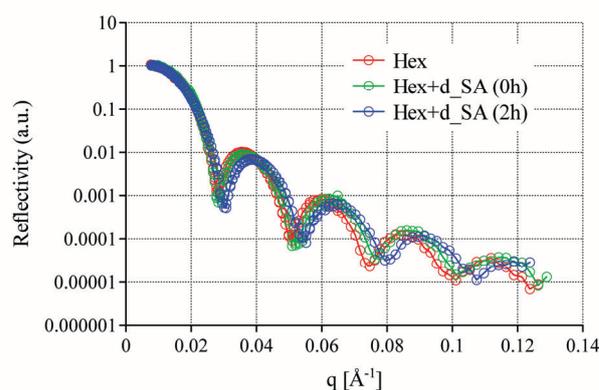
(a) With stearic acid
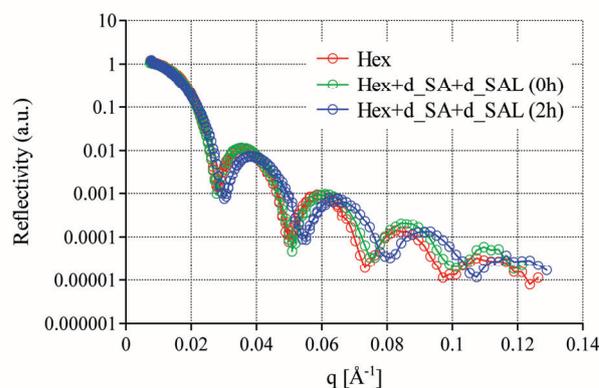
(b) With stearic acid and stearyl alcohol

Fig. 1   Neutron reflectivity profiles for the interface between Cu substrate and lubricant.

In addition, the friction tests were conducted under the lubricants only with stearic acid and with both of stearic acid and stearyl alcohol. For the friction test, an atomic force microscope was used owing to its higher sensitivity for the coefficient of friction of adsorption layer. As a result, a lower coefficient of friction was obtained when two were mixed than when only stearic acid was mixed in the base oil. These results suggested that the mixing of multiple kinds of additives may further promote the adsorption, bringing lower friction characteristics.

R2075

CO12-9   Multi-element neutron activation analysis of selected Japanese food samples by meutron activation analysis

M. Fukushima[1], T. Maeda[1], Y. Iinuma [2]

[1]Faculty of Sciences and Engineering, Ishinomaki Senshu University

[2]Institute for Integrated Radiation and Nuclear Science, Kyoto University

INTRODUCTION: It is important to obtain multi element levels in food samples for nutritional purposes. For the analysis of multi elements in food samples, atomic absorption spectrometry (AAS) and induced coupled plasma spectrometry (ICP-AES) are widely used after pre-treatment of acid extraction or acid digestion. Though complete acid digestion is needed for obtaining total levels of elements in food samples, it is not easy by the presence of high concentrations of lipids, polysaccharides, *etc*. preventing acid digestion. For eliminating this problem, neutron activation analysis (INAA) was used for multi elements analysis of Japanese food samples. Wild plants have played an important role as ingredients especially in mountain areas in Japan from long time ago. Unlike vegetables grown in the field, it is known wild plants grown in mountains accumulate specific elements in them. Several species of wild plants were collected from small areas and analyzed elements by INAA.

EXPERIMENTAL: Samples are shown in Table 1.

Table 1.   Wild plant samples

| Wild plants (Japanese name)	Collected areas
Kogomi	Akita Pref., Marumori*, Tome*
Sidoke	Yamagata Pref.
Hosta (Urui)	Fukushima Pref.
Bracken (Warabi)	Ibaraki Pref.
Udo	Akita Pref., Ichihazama*
Aralia elata (Taranome)	Yamagata Pref.
Mizu	Ichihazama*
Wasabi	Ichihazama*
Japanese knotweed (Itadori)	Ichihazama*
Japanese butter bur (Fuki)	Ichihazama*
Water drop wort	Kahoku*

*Miyagi Pref.

Wild plants were collected in April-May, 2020. Samples were washed with tap water, separated edible parts, freeze dried, and pulverized for dried powder samples. NAA was done by two different conditions according to nuclides for the interest.   1) One portion of samples was irradiated for 1-1.5 min in TcPn site.   After 3 minutes decay, gamma spectrum was measured for 10 minutes by Ge detector with CSS.   Levels of Br, Ca, Cl, I, K, Mg, Mn, Na, and V were analyzed using ^{80}Br, ^{49}Ca, ^{38}Cl, ^{128}I, ^{42}K, ^{27}Mg, ^{56}Mn, ^{24}Na, and ^{52}V.   2) Another portion of samples was irradiated for 1 hour, and gamma spectrum

was measured for 20 minutes after 1 month decay for analyzing Ag, Co, Cr, Cs, Fe, Rb, Sc, Se, and Zn using ^{110m}Ag, ^{60}Co, ^{51}Cr, ^{134}Cs, ^{59}Fe, ^{86}Rb, ^{46}Sc, ^{75}Se, and ^{65}Zn, respectively.   NAA method used was validated using NIST SRM 1570a Spinach Leaves, NIST SRM 1566b Oyster Tissue, NIST SRM 1575 Pine Needles, and NIST SRM 1573a Tomato Leaves.

RESULTS: Six different species of wild plants were collected from small area of Ichihazama, Miyagi on same day.   Mizu accumulated Mg, Ca, and Fe comparing other species, Wasabi did Rb and Fe, Japanese butter bur did Ca and Rb in them.   Those tendencies are thought to be their characteristics, since those six species were growing in small areas.

Elemental levels of Udos collected from five different areas (results of Ishinomaki, Iwadeyama, and Unnan were obtained in 2019) were compared each other.   are shown in Fig. 1, and Mn, Rb, and Zn levels differed much each other.   Also, elemental levels of Bracken from Tsukuba were compared with those from Ishinomaki and Kahoku in 2019, and shown in Fig. 2.   Levels of Mn differed each other in three areas.
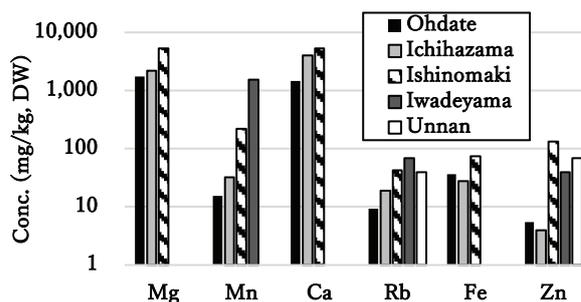
Fig.1 Elemental levels of Udos collected from five different areas.
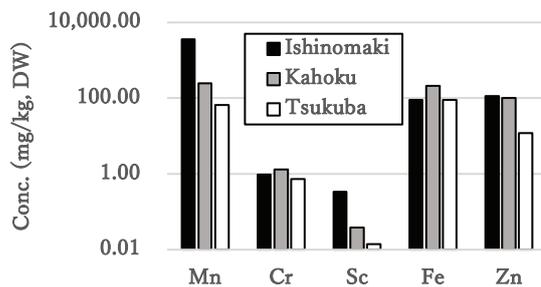
Fig. 2 Elemental levels of Brackens collected from two different areas.

R2085

Analyzing the Texture of Roof-tile toward Detailed Provenancial Studies of Excavated Ceramics by NAA

M. Tomii, K. Takamiya[1], H. Yoshii, M. Kidachi[2], A. Ito, J. Sterba[3], M. Shinoto[4], Y. Chiba

Graduate School of Letters, Kyoto University
[1]*Institute for Integrated Radiation and Nuclear Science, Kyoto University*
[2] *College of Letters, Ritsumeikan University*
[3]*Atominstitut, TU Wien*
[4]*Institut für Ur- und Frühgeschichte und Vorderasiatische Archäologie, Universität Heidelberg*

INTRODUCTION: Aiming to establish the procedures to archaeologically identify local groups for production of ceramics (pottery and roof-tiles) in historical times in Japan, a collection of excavated roof-tiles is analyzed. Considerable amount of fragmented roof-tiles were excavated at the archaeological site in the campus of Kyoto University (KU) which had been roofed, prior to the occupation of KU, on the temporal house for the garrison from *Tosa* domain (today's Kochi prefecture) in the middle of 18th century. This collection includes many pieces that have stamp impressions indicating that they had been made by the tile-makers within *Tosa* region [1]. Despite difference in potter's names written in the impressions, the technological difference among tiles in the collection has been improbable to recognize.

In order to archaeologically understand the local ceramics production system in historical times with high resolution, this study tries to check whether the difference in stamp impressions, suggesting different production groups, corresponds with the texture of tiles in detail. In the present work, the elemental compositions of the tile samples have been determined by neutron activation method.

EXPERIMENTS: Conventional INAA was applied to determine the elemental composition of tile samples. The tile sample was drilled into a fine powder (Fig.1) and enclosed in a polyethylene bag [2]. The bag was covered with another polyethylene bag to suppress contamination in handling. Each sample was neutron irradiated at Pn-3 of KUR (1 MW) for 90 seconds to detect short-lived nuclides. And all samples were irradiated at Pn-2 (1 MW) for 1 hour to determine long-lived ones. The comparative standards (JR-3, JB-1b) were irradiated with the same condition. The gamma-ray spectrometry of the irradiated samples for short-lived nuclides had been performed just after the irradiation several times, repeatedly. The samples for long-lived ones were measured three weeks after the irradiation. The photo-peak analysis was performed by using Fitz-Peaks [3]. Concentrations of elements included in the samples were estimated by comparison of the intensity of gamma-rays between the comparative standard and tile samples.

RESULTS: Concentrations of eight elements (Na, Mg, Al, K, Mn, La, Sm and Th) in the roof-tile sample "KS92-277B" were determined by analyzing photo peaks of short half-lived nuclides. The results are listed in Table 1. Concentrations of Na and La were weighted average values since multiple photo peaks of ^{24}Na and ^{140}La were detected. Concentration values estimated for the multiple photo peaks correspond with each other, and the validity of the analysis was confirmed. Estimation of the elemental concentrations for long-lived nuclides and other samples will be performed in the near future, and elemental composition will be compared each other to find out the index elements which shows the specific characteristics of the tiles.

Table 1 Concentrations of eight elements determined for the roof-tile "KS92-277B".

Element	Concentration (μ g/g)		
Na	9.41E+00	$\pm$	4.8E-02
Mg	6.88E+02	$\pm$	1.3E+02
Al	3.67E+04	$\pm$	4.5E+02
K	6.17E+05	$\pm$	3.0E+04
Mn	1.49E+02	$\pm$	3.1E+00
La	7.26E+02	$\pm$	3.8E+01
Sm	1.37E+02	$\pm$	1.3E+01
Th	2.07E+01	$\pm$	3.8E+00

Fig. 1 Sampling with drilling on the broken side of the excavated roof-tile in the site in KU campus, the other side of which has a stamp impression indicating the symbol of the maker in the mid-18th century.

REFERENCES:
[1] Y. Chiba *et al.*, *Annual Report of Archaeological Researches in KU sites for 1992*. (1995) 65-125.
[2] J. Sterba, *J. Radio. Nucl. Chem.*, **316** (2018) 753-759
[3] J. Fitzgerald, FitzPeaks Gamma Analysis and Calibration Software, https://www.jimfitz.co.uk/fitzpeak.htm

R2096

CO12-11　　Development of high-count rate two-dimensional neutron detector system

S. Sato, K. Mori[1], Y. Yoshino[1], T. Seya, T. Otomo, H. Oshita

High Energy Accelerator Laboratory, KEK
[1] Institute for Integrated Radiation and Nuclear Science, Kyoto University

INTRODUCTION: Most of the neutron detectors currently in use are ^{3}He gas detectors, and some neutron scintillator detectors are used to obtain high counting rate and high position resolution. In this study, the LiTA system [1] has been developed as a high counting rate two-dimensional detector system. However, it is expensive and difficult to use, and it has been not widely used. Therefore, we have developed an ADCnet64 system as a low-cost, simple using, and high-counting-rate two-dimensional neutron detector system instead of the LiTA system. The performance of the ADC net64 system was evaluated using the B3 port of KUR.

EXPERIMENTS: The ADCnet64 system is a readout circuit for high-speed scintillators. It has 64 channel high-speed analog to digital converters (ADCs) with 10 bits 80 MHz sampling rate to read a 5 cm square 8×8 multi-anode type photomultiplier tube. Although the ADCnet64 system is inferior to the LiTA system in performance, the similar data are obtained by fewer circuits and easy way. Figure 1 shows a two-dimensional graph using the ADCnet64 with the Cd "KENS" characters affixed. As a neutron scintillator, 1 mm thick ^{6}Li glass was used. Figure 2 shows the pulse waveform of several scintillators. These light emission times are compared with a ^{6}Li scintillator. In this case, full width at half maximums were about 20 ns for APLF, 20 ns for Ce-APLF2019, 30 ns for Ce-APLF2020, and 40 ns for 6Li. In addition, the tail of after-blow of 60 ns for Ce-APLF2019, 120 ns for Ce-APLF2020, and 1000 ns or more for 6Li were confirmed.

RESULTS: We have developed the ADCnet64 system with a low-cost, simple, high-counting-rate, and two-dimensional neutron detector. We have evaluated its performance using the B3 port at KUR.
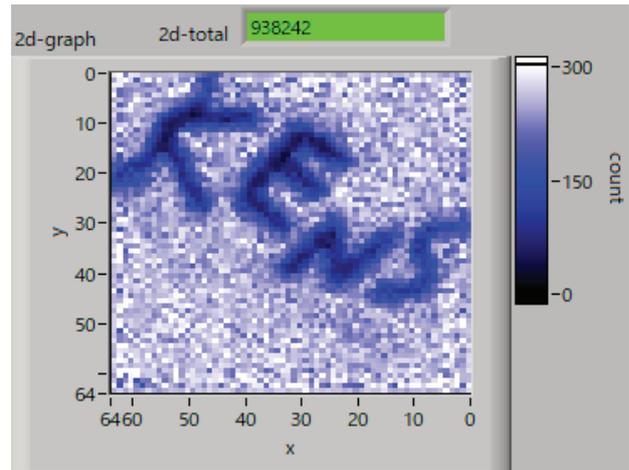

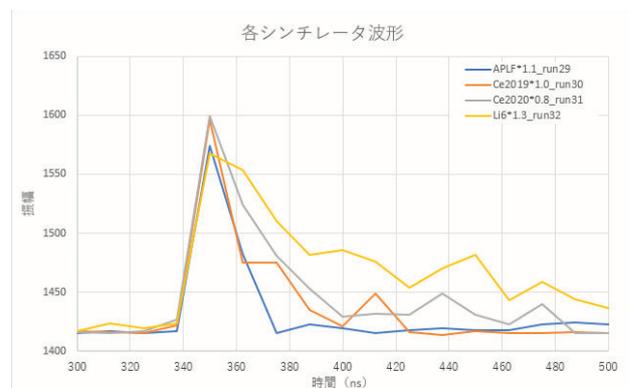Fig. 1.　Two-dimensional graph using the ADCnet64 with the Cd "KENS" characters attached.

Fig. 2.　Pulse waveform of several scintillators.

REFERENCES:
[1] S. Satoh, UCANS-V 2015, DOI 10.1393/ncc/i2015-15197-7.

R2106

A response of inner-through type ionization chamber to ^{133}Xe

A. Yunoki, H. Yashima[1], R. Okumura[1], T. Yamada[2]

National Metrology Institute of Japan, National Institute of Industrial Science and Technology
[1]KURNS
[2]Kindai University Atomic Energy Research Institute

INTRODUCTION: The national metrology institute of Japan (NMIJ) calibrates a response of equipment for monitoring a radioactivity in gaseous effluents. The response is obtained by dividing the indication of the equipment by the activity per unit volume. It can be determined by using an inner-through type ionization chamber (Ohkura ionization chamber: type I-4096 01/06) which is calibrated by a set of proportional counters. ^{85}Kr is used for calibrating the monitoring equipment [1-3]. For monitoring purpose, an energy dependence of the equipment should be assessed. ^{133}Xe and ^{41}Ar are useful, however, it is difficult to purchase them commercially. Therefore, we planned to produce them and perform the assessment. We tested the response of the inner-through type ionization chamber using ^{41}Ar produced in KUR-SLY last year [4]. This year, we tested the response using radioactive xenon gas.

SOURCE PREPARATION: The source of radioactive xenon was produced by activating stable xenon (^{128}Xe, ^{130}Xe, ^{132}Xe, ^{134}Xe, ^{136}Xe) with irradiating thermal neutron. A xenon gas diluted by P-10 was poured to a small vessel of acrylic resin whose volume was 62 cm^3. A pressure of the gas was 100 kPa. Then, the vessel was placed at the bottom of the KUR-SLY operating at 1 MW for 60 s. The nominal flux of the thermal neutron was 7.84×10^{11} [n^{-1} s^{-1} cm^{-2}]. The ^{133}Xe of 17.4 kBq was produced through ^{132}Xe (n, γ) ^{133}Xe reaction, while impurities of ^{129m}Xe, ^{131m}Xe, ^{133m}Xe, ^{135m}Xe, ^{135}Xe and ^{137}Xe were also produced. The radioactive xenon gas was then transported to Kindai University Atomic Energy Research Institute where a measurement system was temporally installed. The ^{41}Ar was also produced in KUR and used in the test.

MEASUREMENTS: A particle emission rate of radioactive xenon gas was assessed by using a set of proportional counters connected in series. Conventional pulse counting electronics were connected to the counters. The designs of the counters are the same except for their length. To eliminate distortion of counts near both ends of the counter, the net count rate was used which was obtained by subtracting a count rate obtained by a shorter counter from that obtained by a longer counter. The particle emission rate can be easily converted to activity for ^{85}Kr and ^{41}Ar. The pure ^{85}Kr is commercially available and pure ^{41}Ar can be produced in KUR. However, pure ^{133}Xe is difficult to obtain because pure stable ^{132}Xe is difficult to prepare and there exist impurities (^{129m}Xe, ^{131m}Xe) of longer life. Therefore, results of this test are not for an activity per unit volume but for a particle emission rate per unit volume including from impurities.

RESULTS: Fig. 1 shows pulse height spectra of signals obtained from the proportional counters whose volumes are 100 cm^3 (LL), 60 cm^3 (M), 44 cm^3 (S), 30 cm^3 (SS). A continuous spectrum of beta particles from ^{133}Xe are observed with several peaks of internal conversion electrons and Auger electrons due to impurities. Fig. 2 shows a pulse count rate as a function of a volume of proportional counter. A count rate per unit volume is derived from an inclination of approximate straight line obtained by the least square method. It was 35 s^{-1} cm^{-3}. The output of inner through ionization chamber flown by the radioactive xenon gas was 13.7 pA. Then, the response of 0.39 pA (s^{-1} cm^{-3})$^{-1}$ was obtained.
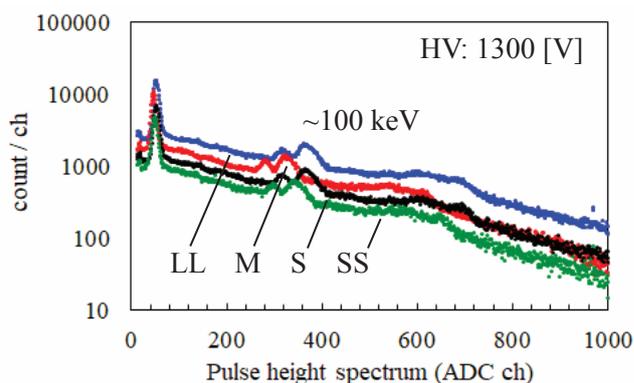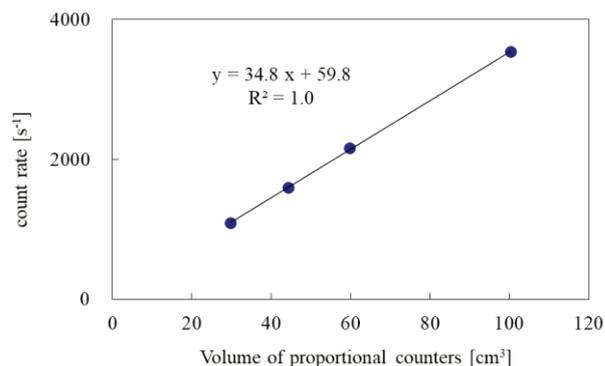

Fig. 1. Pulse height spectra of signals.

Fig. 2. Count rates as a function of a volume of proportional counter.

As for the response test using ^{41}Ar, we inserted lead shield of 10 cm in thickness between each proportional counter and the chamber. The production of ^{41}Ar and measurements were performed similarly.

REFERENCES:
[1] A. Yunoki, et. al., Applied Radiation and Isotopes, Vol. 68 (2010) pp.1340-1343.
[2] M Unterweger, L Johansson, L Karam, M Rodrigues and A Yunoki, Metrologia 52 (2015) S156-S164.
[3] A. Yunoki, et. al., Applied Radiation and Isotopes, Vol. 134 (2018) pp.325-328.
[4] A. Yunoki, et. al., KURNS Progress Report 2019, ISSN 2434-9488, CO12-5 (31059).

R2116

CO12-13   Study of Isotope Separation via Chemical Exchange Reaction

R. Hazama, T. Yoshimoto, A. Rittirong, Y. Sakuma[1], T. Fujii[2], T. Fukutani[3], Y. Shibahara[3], A. Sunaga[3]

*Graduate School of Human Environment, Osaka Sangyo University*
[1]Laboratory for Advanced Nuclear Energy, Tokyo Institute of Technology,
[2]Graduate School of Engineering, Osaka University
[3]Institute for Integrated Radiation and Nuclear Science, Kyoto University

INTRODUCTION: Chemical isotope separation for calcium and lithium has been studied by liquid-liquid extraction (LLE) with DC18C6 crown-ether [1, 2]. This report describes how two important factors of distribution coefficient (D) and separation factor (α) behave in terms of the aqueous phase concentration and different solvent of water and 12M HCl.

EXPERIMENTS: Chemical Isotopic exchange occurs according to the following chemical exchange reaction:

$$^{40}Ca^{2+}_{(aq)} + {}^{48}CaL^{2+}_{(org)} \rightarrow {}^{48}Ca^{2+}_{(aq)} + {}^{40}CaL^{2+}_{(org)} \qquad (1)$$
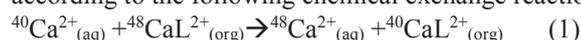
, where L represents macrocyclic polyether(18-crown-6). Various concentrations ranging from 10% to 30% (w/w) $CaCl_2$ and LiCl was used, with/without the addition of 0.3%, 3%, and 30% 12M HCl, and organic solution (0.07M DC18C6 in chloroform) were mixed by a magnetic stirrer for 1 minute and separated with a constant standing time of 10 minutes. Ca and Li concentration measured by AAS (Shimadzu AA-6800). The isotopic analysis performed by ICP-MS (Agilent 7900) (Fig 1, 2). It is noted that the calcium isotope analysis by ICP-MS is in progress.
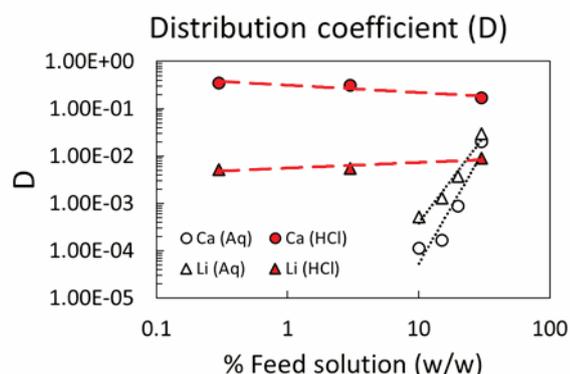

Fig 1. Distribution coefficient (D= [ion]$_{Org}$ / [ion]$_{Aq}$) of LLE: Preliminary.

    The distribution coefficient (D) in aqueous solvent significantly decreases when the feed concentration is reduced. On the other hand, 12M HCl solvent improved and maintained the affinity of ion-crown complex, especially on the calcium extraction by LLE to the higher

extractable salt. At 30% (w/w) of $CaCl_2$, it is found to be about nine times higher by using 12M HCl as a solvent. The result on acidity solvent corresponded to the study on crown-ether resin for calcium isotope separation using the chromatographic method to absorb calcium ion to crown-ether resin [3]. However, the distribution coefficient (D) on lithium was found to be slightly lower by using HCl solvent. The lithium single stage separation factor (α) analyzed by ICP-MS provided 1.008 ± 0.004 and 1.009 ± 0.003 for 12M HCl and an aqueous solvent, respectively.
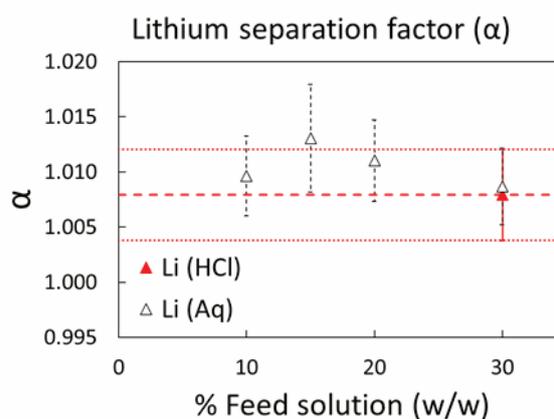

Fig 2.   Lithium single stage separation factor (α= [^6Li/^7Li]$_{Org}$/[^6Li/^7Li]$_{Aq}$): Preliminary.

RESULTS: It is noted that the recovery of cation content significantly influences a scale-up on mass production progress of isotope enrichment. With the current setup, we found that the formation of ion-crown complex is reduced, where the feed concentration is decreased for aqueous solvent. However, the formation of ion-crown complex is significantly increased with the addition of 12M HCl solvent, especially in the case of calcium. The requirement for the multi-stage iteration to obtain about ten times enrichment of ^{48}Ca is relaxed with the current improvement utilized by acidity solvent. It requires several thousand times for aqueous solvent, but it is only 1400 times if we utilize 12M HCl as a solvent. For comparison, the same crown-ether was used for both Ca and Li in this study, but the optimization of crown-ether, solvent, molar ratio between these two, temperature, etc is required to improve mass production cost-effectively.

REFERENCES:
[1] R. Hazama *et al*., KURRI Progress Report 2017, 104.
[2] R. Hazama *et al*., KURNS Progress Report 2019, 282.
[3] S. Nemoto et al., Journal of Nuclear Science and Technology 2012, 49.4: 425-4

R2119

CO12-14   Beam test of radiation detectors for a muon-electron conversion search experiment, DeeMe

M. Aoki, N. Abe[1], Y. Higashino, H. Ikeuchi[2],
K. Komukai[2], D. Nagao, H. Natori[4], Y. Seiya[2,3],
K. Sugita, T. Takahashi[1], N. Teshima[2,3], T. Uematsu[2]
and K. Yamamoto[2,3]

School of Science, Osaka University

[1]*Kyoto University Institute for Integrated Radiation and Nuclear Science, Kyoto University (KURNS)*

[2]*Faculty of Science, Osaka City University*

[3]*Nambu Yoichiro Institute of Theoretical and Experimental Physics (NITEP), Osaka City University*

[4]*Institute of Materials Structure Science, KEK*

INTRODUCTION: Charged-lepton flavor violation (CLFV) process such as $\mu \rightarrow e\gamma$, μ-e conversion, τ-CLFV decays are heavily suppressed in the standard model of particle physics (SM). However, in the most of the models beyond SM, it is considered to occur with a strength that can be reached in the coming experiments. DeeMe is one of experiments that aims to search for μ-e conversion in nuclear field [1] at a level of 10^{-13} of the branching ratio in the single event sensitivity. It uses high-power high-purity pulsed proton beam from J-PARC RCS. The detector of DeeMe should be operational after $\mathcal{O}(\mu s)$ from a burst of particles (100 GHz/mm^2) produced by the proton pulse.

In order to solve this prompt-burst issue, a multi wire proportional chamber (MWPC) with high-voltage switching technique was successfully developed [2]. Since then, the improvements of the MWPC such as reducing the delayed false signals have been performed. Because that it is critically important to improve the overall performance of the momentum-measuring system, we decided to extend our development beyond the MWPC including a fiber tracker that can provide extra information to reduce the bad impact from the delayed false pulses.

We also made use of the burst-beam test technique we had developed with a LINAC at KURNS for the development of a beam-profile monitor that can be used in the pulsed-beam facilities.

EXPERIMENTS: Three independent measurements/tests by using the burst-beam test technique were performed at the LINAC at KURNS. One is the further test of the MWPC, second is the test of the plastic-scintillation fiber tracker, and the third is a test of beam profile monitor.

In the test for the MWPC, the two different geometrical configurations of the MWPC were tested: 3 mm of half-gap and 4 mm of half-gap.

In the plastic-scintillation fiber tracker test, we had tried to understand the nature of unexpectedly delayed signals observed in the SiPM output from the fiber after a prompt burst irradiated. By comparing three different fiber configurations, it was concluded that the cause of delayed pulses is likely to be in the SiPM. Then, we had used a newly developed bias-voltage switching SiPM to see the response of the SiPM against a burst input hoping

that the burst-tolerance of the SiPM could be improved by turning-off the SiPM during the burst input.

The beam profile monitor we are developing is optimized to the pulsed beam line, where the individual beam particles cannot be separated. In order to obtain 2-dimensional beam profile, a small-sized detector head is moved in a grid by an industrial robot. The head should produce a pulse whose amplitude is proportional to the number of beam electrons without contamination from beam muons at 105 MeV/*c*. Figure 1(a) shows the newly developed prototype of the detector head that uses Cherenkov radiation to separate electrons from muons.

RESULTS: The time spectra of the fiber signals read by the switching SiPM for two different switching timings showed that turning-off the SiPM during the burst did not suppress the delayed pulses. The further study aiming to understand the cause of the delayed pulses and to reduce them are ongoing.

Figure 1(b) shows the result of the burst-electron detection performance for the beam profile monitor head tested at the LINAC [3]. The head showed good performance and can be used in the coming beamline commissioning at J-PARC.
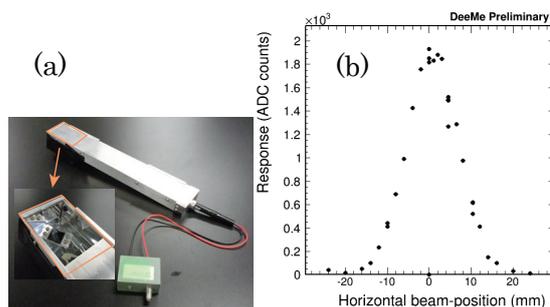

Fig. 1 (a): a detector head of a pulsed-beam profile monitor. (b): profile of a pulsed-beam measured by the Cherenkov detector head at the LINAC.

REFERENCES:
[1] N. Teshima on behalf of the DeeMe Collaboration, "DeeMe experiment to search for muon to electron conversion at J-PARC MLF", in proceedings of NUFACT conference PoS (NuFact2017) 109 (2018).
[2] H. Natori, *et al.*, "A fast high-voltage switching multi-wire proportional chamber", Prog. Theor. Exp. Phys. 2017(2) 023C01 (2017).
[3] K. Komukai, "Development of beam-profile scanning devides for a pulsed beamline", Master Thesis, Osaka City University, March 2021.

CO12-15   Neutron activation analysis of Ar, Cl, Br and I in Pd metal

T. Miura, N. Yoshinaga[1], Y. Iinuma[1] and S. Sekimoto[1]

National Metrology Institute of Japan, AIST
[1]Institute for Integrated Radiation and Nuclear Sciences, Kyoto University

INTRODUCTION: National Metrology Institute of Japan (NMIJ) is responsible for developing certified reference materials and for establishing the traceability of SI (The International System of Units) on chemical metrology in Japan. To establish SI traceability, the primary method of measurements should be applied to the characterization of the certified reference materials. Recently, neutron activation analysis using comparator standard is recognized as a potential primary ratio method [1]. Despite the potential of neutron activation analysis as primary ratio method, the evaluation of the measurement uncertainty is required in any analysis. In general, there are three main components of uncertainty in neutron activation analysis, that is, sample preparation uncertainty, neutron flux homogeneity, and gamma ray measurement uncertainty. Usually, flux monitor is used to correct the neutron flux in-homogeneity. However, although the flux monitor can correct the neutron flux variation using the count rate of the known amount of the monitor nuclide, it does not reflect the neutron flux of the actual sample. The most practical method to eliminate neutron flux in-homogeneity and to improve gamma ray measurement uncertainty is an internal standard method [2, 3]. For the development of primary inorganic standard solution as national standard, the purity of starting material has to be determined. The high purity Pd metal was candidate starting material for preparation of Pd standard solution as national standard of Japan. The several trace analytical methods including neutron activation analysis, were used for purity determination of the high purity Pd metal. In this work, we presented that capability of instrumental neutron activation analysis for determination of Ar and halogens in high purity Pd metal.

EXPERIMENTS: The high purity Pd metal was purchased from Tanaka precious metals. The informative purity value of the Pd metal was 99.9 %. The ambient air in pre-cleaned 2 mL volume of Polyethylene vials were used as Ar calibration standard. The volumes of polyethylene vials were calibrated by weighing mass of pure water prepared from Mill-Q Advance pure water system filled in each vial. The calibration of volume Mettler Toredo XP205 semi-micro balance was used for volume calibration. NMIJ CRM 3802a Cl standard solution, NMIJ CRM 3808a Br standard solution and NMIJ CRM 3810a I standard solution were used for used as Cl, Br and I calibration standard, respectively. The standard solutions were added on filter papers to prepare the calibration standard for Cl, Br, and I analysis. The calibrated polyethylene vials, Cl, Br, and I calibration standard were heat sealed into polyethylene bags. Thirty mg of the Pd metal samples were used for Ar, Cl, Br and I analysis. The neutron irradiations were performed by KUR (Kyoto University Research Reactor) Pn3 (thermal neutron flux: 4.7×10^{12} cm^{-2}s^{-1}) for 1 min. The γ ray measurement system consisted of an ORTEC GEM 30-76-LB-C-HJ Ge detector and a multichannel analyzer SEIKO EG & G MCA 7.

RESULTS: In this experiment, Ar, Cl, Br and I in the high purity Pd metal sample could not be detected by instrumental neutron activation analysis. Therefore, the detection limits of Ar, Cl, Br and I in the high purity Pd metal sample were estimated from the count rate of energy region of γ rays emitted by induced radioactive nuclides. The estimated detection limits were shown on Table.

Table Analytical results of Ar, Cl, Br and I in high purity Pd metal

	Detection limits, g/g
Ar	$< 4 \times 10^{-6}$
Cl	$< 3 \times 10^{-6}$
Br	$< 2 \times 10^{-6}$
I	$< 0.5 \times 10^{-6}$

REFERENCES:
[1] R.Greenberg, P. Bode, E. De Nardi Fernandes, Spectrochim. Acta B, 66 (2011) 193-241.
[2] T. Miura, K.Chiba, T. Kuroiwa, T. Narukawa, A.Hioki, H. Matsue, Talanta, 82 (2010) 1143-1148.
[3] T. Miura, R. Okumura, Y. Iinuma, S. Sekimoto, K. Takamiya, M. Ohata, A.Hioki, J. Radioanal. Nucl. Chem., 303(2105), 1417-1420.
[4] NuDat 2, National Nuclear Data Center in Brookhaven National Laboratory, https://www.nndc.bnl.gov/nudat2/index.jsp

R2154

CO12-16 **Evaluation of Structural Vacancies in Icosahedral Cluster Solids using Positron Annihilation**

M. Yamamoto[2], R. Nakajima[3], K. Kitahara[1], A. Yabuuchi[3], N. Oshima[4], I. Kanazawa[2], A. Kinomura[3], K. Kimura[1]

[1]*Department of Advanced Materials Science, The University of Tokyo*
[2]*Department of Physics, Tokyo Gakugei University*
[3]*Institute for Integrated Radiation and Nuclear Science, Kyoto University*
[4]*National Institute of Advanced Industrial Science and Technology (AIST)*

INTRODUCTION: Stable Al-based icosahedral quasicrystals of multinary aluminium-transition metal alloys are known to exhibit semiconductor-like and even insulator-like electronic transport properties [1]. It has been suggested that the semiconductor-like properties might be interpreted by the combnination of a pseudogap around the Fermi energy and localization tendency. One of origins of the pseudogap at E_F in quasicrystals might be ascribed to a Hume-Rothery like mechanism, namely the scattering of electrons around E_F by planes of pseudo-Brillouin zone constructed from the most intense diffraction peaks. So far, the origin of the pseudogap is not confirmed. Janet and de Boissien [2] proposed a cluster model to explain the properties and the stability of quasicrystals. The icosahedral structure is based upon clusters that contain a number of electrons which stabilizes the structure of atomic aggregates. Mayon *et.al.* [3] proposed a possible explanation for the unusual transport properties of Al-based quasicrystals in terms of hopping processed between wave functions mainly localized inside icosahedral clusters. Kimura *et.al.* [4] have discussed the importance of vacant centers of the Al icosahedral clusters in the anomalous transport properties and stabilities of Al-based quasicrystals. They have shown that 12-atoms Al icosahedra with a vacant center have a covalent bonding nature, while 13-atoms with a center atom have a metallic bonding nature. Positron annihilation method is powerful one for detecting structural vacancies of icosahedral quasicrystals [5]. Recently Kimura and coworkers [6] have done positron annihilation measurements of the positron lifetime, coincidence Doppler broadening (CDB), and depth profiling by slow positron beams for 1/1 AlReSi approximant crystals. They showed that 1/1 AlReSi approximant crystal has structural vacancies in the order of 10^{-3}, which are identified to be center sites of the first shell of icosahedral clusters, and then found that the structural vacancy density of metallic 1/1 AlReSi with less Re is lower than that of non-metallic AlReSi with more Re. These results are consistent with a hypothesis by Kimura *et.al.* [4] and accelerate further investigation of the relationship between structure, bonding nature, and electrical properties for Al-based quasicrystals and approximant crystals, leading to better understanding of physics behind quasicrystals and approximant crystals in terms of the proposed metallic-covalent binding conversion which occurs according to the occupation and vacancy of the center sites of the Al icosahedral clusters.

EXPERIMENTS and RESULTS:
Figure shows X-ray diffraction patterns of quasicrystals $Al_{71}Pd_{18}Ru_{11}$ (upper) and $Al_{71.5}Pd_{18}Ru_{10.5}$(middle), and one calculated by the structural model(lower). By using the slow positron beam, we have estimated the change in S-parameter with positron-incident energies in 2/1 approximant crystal AlPdRu, and 1/0 approximant crystal AlPdRu.
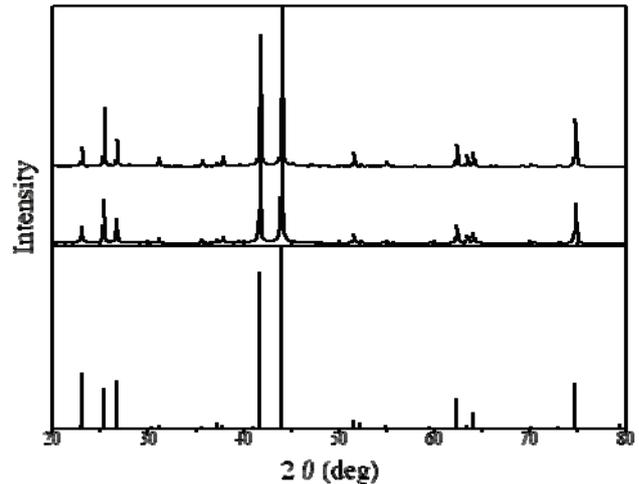

Figure X-ray diffraction patterns of the samples.

We have measured the change of S-parameter of quasicrystal AlPdRu, 2/1 approximant crystal AlPdRu, and 1/0 approximate crystal AlPdRu, due to the positron incident energy. These results show that the density of structural vacancies is the highest in quasicrystal AlPdRu, the second highest in 2/1 approximant crystal, and the lowest in 1/0 approximant crystal. These results are consistent with ones of positron lifetimes of these three samples by slow positron beams (unpublished data). Furthermore, the present results seem to be reasonable from the standpoint of the metallic-covalent bonding conversion which occurs according to the occupation and vacancy of the center sites of the Al icosahedral clusters. We have also done the coincidence Doppler broadening spectra of these three samples. To identify the positron trapping sites in these samples, the core electron momentum distribution of the samples was measured. Experimental results suggest strongly that the trapping sites of quasicrystal AlPdRu, 2/1 approximant crystal AlPdRu, and 1/0 approximant crystal AlPdRu seem to be similar, and are surrounded by Al or Ru.

REFERENCES:
[1] K. Kimura and S. Takeuchi,in Quasicrystals:The State of Art, 2nd ed.,D.P. Divincenzo and P.J. Steinhart,eds.,(World Scientific, Singapore, 1999) pp.325-309.
[2] C. Janot and M.de Boission, Phys. Rev. Lett. **72** (1994) 1674.
[3] D. Mayou et al. Phys. Rev. Lett. **70** (1993) 3915.
[4] K. Kimura et al., J. Solid State Chem. **133** (1981) 302.
[5] I. Kanazawa et al., Phys. Rev. Lett. **79** (1997) 2269.
[6] K. Yamada et al., Philog. Mag. **98** (2018) 107.

R2166

CO12-17　　Basic experiment for nuclear reactor power monitoring with heat-resistant self-powered gamma ray detector

K. Okada, A. Fushimi, Y. Sato, Y. Murakami, S. Sekimo-to[1], T. Ohtsuki[1], Ryo Okumura[1]

Center for Technology Innovation – Decarbonized Energy, Research and Development Group, Hitachi, Ltd.
[1] *Institute for Integrated Radiation and Nuclear Science, Kyoto University*

INTRODUCTION: Conventionally, thermal neutron measurements have been used for nuclear power monitoring in current commercial nuclear reactors. Recently, ion chambers, which are gamma ray detectors, have been adopted overseas as part of the monitoring systems. Gamma ray measurements have an advantage that the installation position dependence is small because of the large neutron flux gradients and the small gamma flux gradients in the water gap between fuel elements [1]. However, the applied gamma ray measurement devices and systems have a long time constant.

We have been developing a self-powered gamma ray detector (SPGD) which measures a current value generated by electrons ejected from an emitter by gamma ray irradiation. As the name suggests, this SPGD does not require a power supply. We assumed that SPGDs were placed in a mixed field of neutrons and gamma rays in a commercial reactor core and at high temperature. We manufactured a prototype of the SPGD characterized by the Pb-Bi emitter which has sensitivity for gamma rays and a low melting point [2]. The prototype SPGD could be used at high temperatures such as in the inner reactor core because it remained functional even if the emitter melted. In this study, we used the Kyoto University Research Reactor (KUR) facility to measure the current value at high dose rate and high neutron flux in order to investigate the correlation between the reactor power and the SPGD current value under the conditions of an operating reactor core.

EXPERIMENTS: The experiments were carried out by using the Slant Exposure Tube (SLY) of the KUR facility. The experimental geometry is shown in Fig.1. The SPGD was inserted into the reactor core from the subpool. The SPGD was connected to a picoammeter by a MI (mineral insulated) cable of 30 m and a coaxial cable of 30 m. Measurement data were transmitted from the picoammeter to control a PC with the GPIB interface. The data were collected for three points per second.

The measurement was performed twice at the time of reactor start-up of 0 MW to 1 MW and the time of reactor powering up of 1 MW to 5 MW. The assumed neutron flux around the SPGD was about 10^{12} n/cm^2/s, which is equivalent to 1 % of the neutron environment of the rated power of commercial nuclear reactors. There was a concern that the SPGD could not be extracted from the reactor core because of radioactivation by irradiation at high neutron flux. Thus, the time to set SPGD in the reactor core was limited to within 30 minutes.
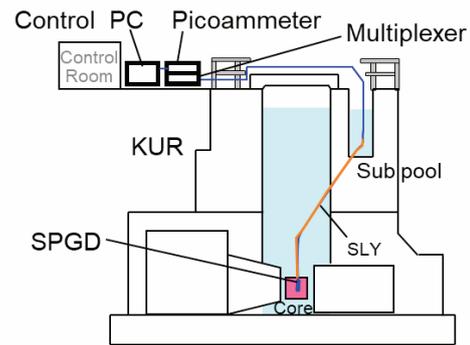

Fig. 1. Experimental set-up of the KUR facility.

RESULTS: Typical measurement results as a time trend of SPGD current value at the time of the reactor start-up are shown in Fig.2. The SPGD current value was increased in response to the rise in the reactor power. The SPGD current value rose after reaching reactor power of 1 MW. The correlation between the reactor power and the SPGD current value was investigated using this result (Fig.3). The SPGD current value at 1 MW was spread over a wide range. The reason was that the SPGD current value continued to rise even after the reactor power had reached 1 MW. This suggested that there might be a time lag before the reactor power was reflected in the SPGD current value.
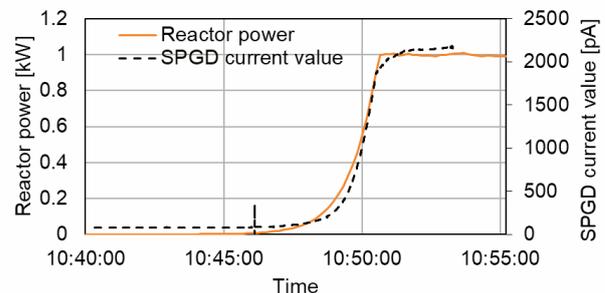

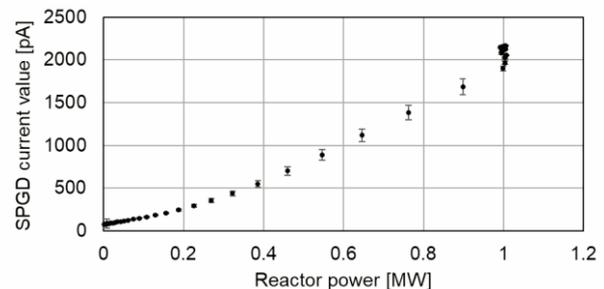Fig. 2.　Time trend of the reactor power and the current.

Fig. 3. Correlation between reactor power and SPGD current value.

REFERENCES:

[1] W. Harfst, IWG-NPPCI--84/1(1985).

[2] K. Okada, et al., Abstract of 2020 Annual Conference of Fundamentals and Materials Society, IEE Japan (2020).

R2168